ADVANCED FUNCTIONAL MATERIALS
www.afm-journal.de

Highly Conductive Nanocomposites with Three-Dimensional, Compactly Interconnected Graphene Networks via a Self-Assembly Process

Chao Wu, Xingyi Huang, Genlin Wang,* Libing Lv, Gan Chen, Guangyv Li, and Pingkai Jiang**

Polymer-based materials with high electrical conductivity are of considerable interest because of their wide range of applications. The construction of a 3D, compactly interconnected graphene network can offer a huge increase in the electrical conductivity of polymer composites. However, it is still a great challenge to achieve desirable 3D architectures in the polymer matrix. Here, highly conductive polymer nanocomposites with 3D compactly interconnected graphene networks are obtained using a self-assembly process. Polystyrene (PS) and ethylene vinyl acetate (EVA) are used as polymer matrixes. The obtained PS composite film with 4.8 vol% graphene shows a high electrical conductivity of 1083.3 S/m, which is superior to that of the graphene composite prepared by a solvent mixing method. The electrical conductivity of the composites is closely related to the compact contact between graphene sheets in the 3D structures and the high reduction level of graphene sheets. The obtained EVA composite films with the 3D graphene structure not only show high electrical conductivity but also exhibit high flexibility. Importantly, the method to fabricate 3D graphene structures in polymer matrix is facile, green, low-cost, and scalable, providing a universal route for the rational design and engineering of highly conductive polymer composites.

1. Introduction

Polymer based materials with high electrical conductivity are highly desirable in practical applications such as electronic devices,[1,2] sensor,[3] actuators,[4] and electromagnetic shielding.[5] Graphene has attracted considerable attention in view of its potential to significantly enhance the electrical conductivity of host polymers with a low loading.[6] Graphene is a two-dimensional and conjugated honeycomb carbon network, which shows many unique and fascinating properties such as giant electron mobility, high thermal conductivity, excellent mechanical flexibility and large specific surface area.[7] Therefore, graphene sheets (GSs) have natural advantages by means of these properties to significantly improve the electrical properties of host polymers. However, a huge challenge still lies in the development of highly conductive graphene-based polymer composites because of the agglomeration tendency of GSs and high contact resistance between GSs in the matrixes. A typical example is graphite nanoplatelet-filled polymer composites. Graphite nanoplatelets can be viewed as the aggregation of GSs. The electrical conductivity of the composites with 3.12 vol% graphite nanoplatelts is only 0.01 S/m.[8]

To improve the dispersion of graphene, a great deal of efforts has been made by the organic group functionalization strategy.[6,9] For example, isocyanate-treated GSs exhibit good dispersion in polystyrene (PS) matrix, and the resulting composites have a conductivity of about 1 S/m with a loading of 2.5 vol%. Ionic-liquid-functionalized GSs can be individuated and homogeneously distributed into polar aprotic solvents, and its PS composite with 4.19 vol% GSs has a conductivity of 13.84 S/m.[10] However, the electrical conductivity of these composites is still far below an expected level, even if homogeneous dispersion is achieved, and there still exists high inter-sheet junction contact resistance between GSs, which arises from these functional groups and polymer matrix between GSs. In addition, these functional groups also damage the electronic conjugation of graphene. The construction of three-dimensional (3D) interconnected graphene networks in polymer matrixes provides a new strategy for fabricating highly conductive graphene composites. 3D graphene network can not only make GSs be uniformly distributed in the polymer matrix, but also significantly reduce the contact resistance between GSs. Although 3D porous graphene films have been prepared by several approaches, such as directional freezing and hydrothermal treatment,[11–13] the attention paid to design and construct 3D structured graphene network in a matrix is scarce so far.[13] Very recently, Cheng's group reported

C. Wu, Dr. X. Huang, Dr. G. Wang, L. Lv, G. Chen, G. Li, Prof. P. Jiang
Department of Polymer Science and Engineering
Shanghai Key Lab of Electrical Insulation and Thermal Aging
Shanghai Jiao Tong University
Shanghai 200240, China
E-mail: xyhuang@sjtu.edu.cn; wanggenlin@sjtu.edu.cn; pkjiang@sjtu.edu.cn

DOI: 10.1002/adfm.201201231

© 2013 WILEY-VCH Verlag GmbH & Co. KGaA, Weinheim

a highly conductive poly(dimethyl siloxane) composites with 3D graphene foams by a template-directed chemical vapor deposition (CVD) method.[14] However, such a method is relatively complex and not easy-operated. Therefore, it still remains a challenge to develop a simple and versatile method to obtain highly conductive polymer composites with 3D graphene networks.

Herein, we present a simple and effective route to fabricate the polymer composites with 3D interconnected graphene networks by using a self-assembly and hot press process. The self-assembly process is driven by mutual electrostatic interactions between graphene oxide (GO) and polymer nanospheres in aqueous phase, indicating that this route is more environment-friendly when compared with the organic solvent processing methods. Different from the graphene structures in polymer matrix formed by the conventional solvent processing method, the resulting 3D graphene network fabricated by our approach can i) realize a uniform distribution of GS without aggregation in polymer matrix and ii) result in GSs directly and tightly contacting between them. As a consequence, the PS composites with 3D graphene structure exhibit a very high conductivity at low graphene loading. In addition, the 3D graphene networks can be constructed in different matrixes by using this approach, such as PS and ethylene-vinyl acetate copolymer (EVA), suggesting a general universality of our current approach.

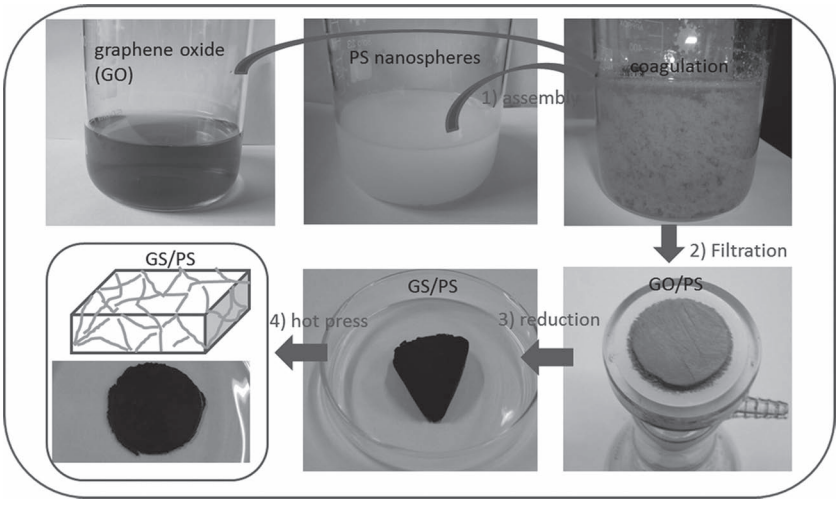

Figure 1. Fabrication process of the polymer composites with 3D interconnected graphene networks.

2. Results and Discussion

2.1. Fabrication of the Graphene-Based Nanocomposites

Graphene has been synthesized by a variety of methods such as CVD, epitaxial growth on SiC, organic synthesis, exfoliation of graphite, and reduction of graphite derivatives (e.g., graphene oxide, GO).[15–17] Currently, graphene-based materials derived from GO can be manufactured on the ton scale at low cost, making GO potentially cost-effective materials for polymer applications.[18] On the other hand, GO is heavily oxygenated, bearing hydroxyl and epoxide functional groups on their basal planes.[19] The presence of these functional groups facilitates GO dispersion in water and polar organic solvent. In this study, GO was used as a reliable and economically feasible source for constructing the 3D graphene networks in polymer matrixs. The preparing procedure of the polymer composites with 3D graphene network is illustrated in **Figure 1**, including four steps. Firstly, PS nanospheres were synthesized via emulsion polymerization and modified by surface grafting of amine groups, which render the sphere surface positively charged. Then, the modified PS nanospheres were assembled with negatively charged GO by electrostatic interactions, resulting in the demulsification of PS spheres and forming a coagulation. GO was uniformly distributed in the gap between the spheres. Under the optimal assembly conditions, almost all the spheres were encapsulated and connected by GO in the coagulation, leaving a transparent aqueous solution. Finally, the resulting coagulation was made into films by filtering and reduced in situ in hydrogen iodide (HI) solution, and then hotly pressed to disk-like plates, resulting in a 3D graphene architecture in polymer matrix. It should be noted that the GO solution and the PS emulsion should be simultaneously added into an empty container under the stirring condition. If GO solution was gradually added into PS emulsion, only partial GO can be assembled with PS spheres, leaving a yellow GO solution, as shown in Figure S1a (Supporting Information).

2.2. Characterization of the Graphene-Based Composites

GO exhibits solution-like dispersion in aqueous phase, as shown in Figure 1. The solution was spin coated on a silica wafer for inspecting the structural features of GO by atomic force microscopy (AFM). A typical AFM image (**Figure 2**a) reveals many free-standing sheets with size of several micrometers and their thickness is about 0.82 nm, suggesting that natural graphite has been exfoliated into monolayer GO. Transmission electron microscopy (TEM) was used to exhibit the morphology and microstructure of GO and as-prepared modified-polystyrene nanospheres. TEM image of GO (Figure 2b) shows the same morphology as the observations from AFM. Figure 2c gives a representative TEM image for PS nanospheres, along with a sphere size distribution. Many colloidal PS nanospheres with diameters ranging from 150 to 220 nm are observed. Notably, the surface of these spheres is very smooth.

In order to examine the electrostatic interaction between the modified nanospheres and GO, the surface charges of nanospheres and GO were measured by zeta potential instrument. As displayed in Figure 2d, the surface of GO is negatively charged (zeta potential = –35 to –55 mV) over the investigated pH range (2–11), in agreement with the reported studies.[20,21] These negative charges originate from the ionization of the carboxylic acid and phenolic hydroxyl groups on the GO

© 2013 WILEY-VCH Verlag GmbH & Co. KGaA, Weinheim

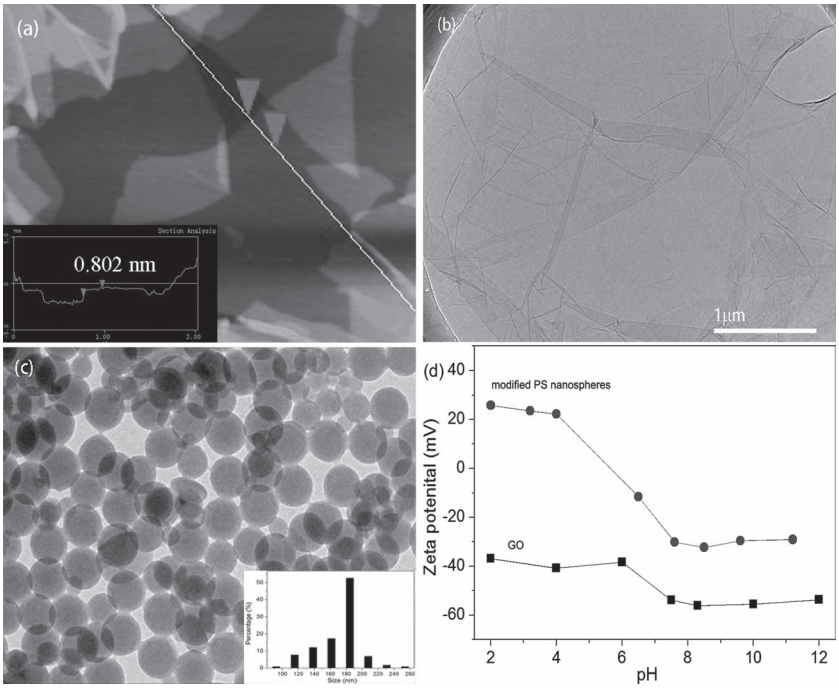

Figure 2. a) Typical AFM and b) TEM images of GO. c) TEM image of the amino-modified polystyrene nanospheres. d) Zeta potentials of GO and the amino-modified nanospheres.

backbone.[21] For the modified nanospheres, the surface charges switch from positive (zeta potential = +26 mV) to negative (zeta potential = –29 mV) with increasing pH value from 2 to 11. In the experiments, we found that the spontaneous aggregates immediately formed once the nanospheres solution was added into the GO solution at pH value of 4, such a phenomenon is not observed at pH value of 10, shown in Figure S1b (Supporting Information), indicating that the electrostatic interaction is the driving force. Additionally, no large aggregates were observed at pH value < 1, possibly owing to protonation of GO. This result suggests that the mutual assembly should be triggered under weakly acidic medium.

It is well known that GO is an electrically insulating materials, which arises from a large amounts of oxygen-containing groups on it basal planes. After removing such groups by a reduction process, the electrical properties of graphene sheets are supposed to be restored, presumably owing to restoration of the graphitic network of sp^2 bonds.[22,23] So far, several reduction methods of GO, such as thermal, chemical, and ultraviolet-assisted reduction, have recently been reported.[24–27] However, the resulting GSs are prone to the irreversible aggregation during the reduction process because of the strong π–π stacking and hydrophobic interactions. Consequently, many of the unique properties of individual sheets are significantly compromised or even unavailable.[28] Thus, GO and modified GO were reduced under a mild reduction condition to remain some functional groups for preparing polymer composites.[29,30] In contrast, the coagulations consisting of GO and PS nanospheres were reduced in high concentration HI solutions for removal of most functional groups on GO. For this approach, the aggregation of GSs did not happen because that the nanospheres can effectively prevent GSs from aggregating. This feature is indeed demonstrated by the field emission scanning electron microscopy (FE-SEM) images of the resultant reduced coagulations. As shown in **Figure 3**, many nanospheres adsorb to the same GS sheet at a low graphene loading. The nanospheres adsorb more GSs with an increase of graphene content. Almost all nanospheres are encapsulated by GSs at the high content. Compared with pristine nanospheres, the graphene-encapsulated spheres exhibit crinkled and rough textures, which are associated with the presence of flexible and ultrathin GSs. Remarkably, no free graphene aggregates and naked PS nanospheres appear in the SEM visualizations even at high content, and the edges of graphene shells are overlapped or linked between the neighboring spheres to form a 3D graphene framework in the coagulations.

In order to evaluate the reduction level of GO, the graphene framework was extracted by removing the PS nanospheres in dimethyl formamide (DMF) solution by ultrasonic treatment. The morphology of the resulting graphene framework is investigated by TEM image. As shown in Figure a4a,b, a graphene network with ripples and wrinkles are observed, but the network structure has no regular pores remained after removal of nanospheres, which is attributed to the collapse of graphene framework under ultrasonic condition. The thermal properties and microstructure of the graphene network was further investigated by thermogravimetric analysis (TGA) Fourier transform infrared spectroscopy (FT-IR), and X-ray powder diffraction (XRD). **Figure 4**c shows the TGA curves of GO and GSs. GO is thermally unstable and starts to lose mass even below 100 °C, which is attributed to the volatilization of stored water in its π–π stacked structure. The major loss appears near 180 °C, which is ascribed to the pyrolysis of labile oxygen-containing groups. For GSs, it is thermally stable and exhibits a minor mass loss (12%), suggesting that most of functional groups on the surface of GO are removed during the HI reduction process. The FT-IR spectra of the GO before and after reduction are presented in Figure 4d. It is clearly observed that almost no absorbance peaks are detected for GSs. For GO, many overlapped absorbance perks are observed, including the distinguished peak at 1740 cm^{-1} representing the carbonyl moieties (C=O) and the peak at 3400 cm^{-1} representing hydroxyl groups. The FT-IR analysis of GO and GSs also demonstrated that the reduction method is effective and can be used to remove most of the oxygen-containing moieties from GO. The collapsed graphene framework was collected and pressed into graphene paper for XRD analysis. As shown in Figure S2a,b (Supporting Information), the XRD patterns of GO only reveal an sharp (002) diffraction peak at $2\theta = 9.6°$, indicating that the natural graphite is oxidized into GO, in agreement with the observation from AFM. After reduction of GO, a broad peak centered at $2\theta = 24.2°$ is detected, corresponding to an interlayer spacing of 0.36 nm. This value is slightly lower than that (0.38 nm) of thermal

© 2013 WILEY-VCH Verlag GmbH & Co. KGaA, Weinheim

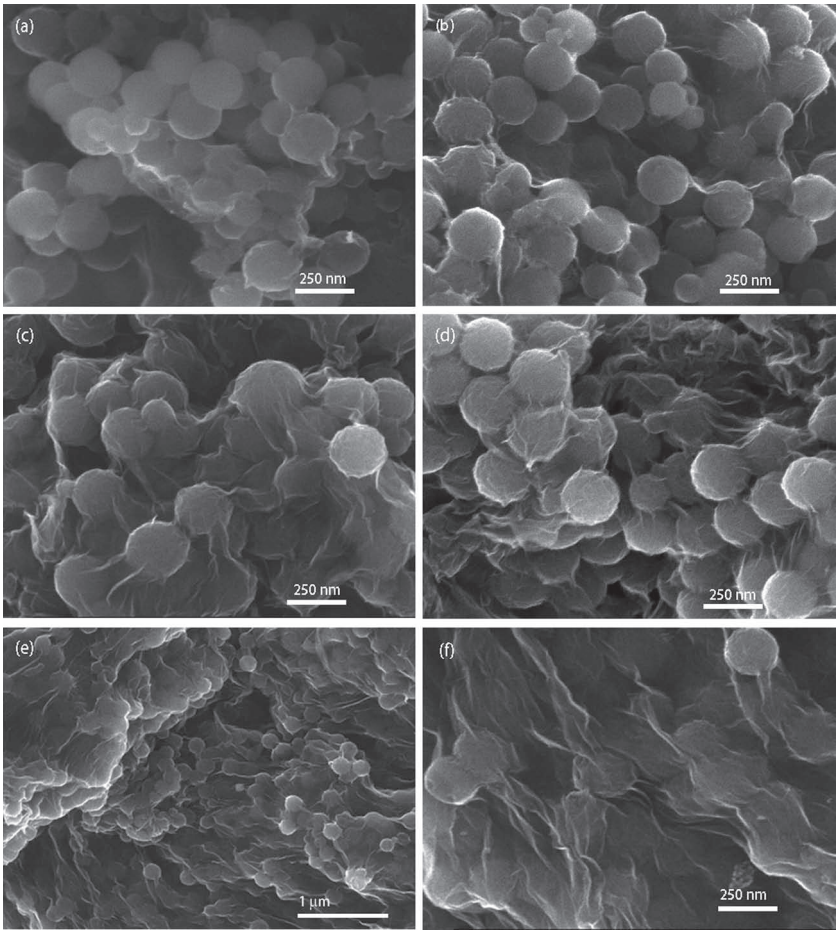

Figure 3. Typical SEM images of the reduced coagulations as a function of GS loading: a) 0.45 vol%, b) 0.91 vol%, c) 2.2 vol%, d) 3.5 vol%, and e,f) 4.8 vol%.

reduced graphene paper,[11] indicating more functional groups were removed.

Raman and UV-vis absorption technologies provide further evidences for the GO reduction. The representative Raman spectra of GO and GSs exhibit two strong major bands, the G-band (the E_{2g} phonon mode of sp^2 carbon atoms) at around 1580 cm^{-1} and D-band (the breathing mode of k-point mode of A_{1g} symmetry) at around 1351 cm^{-1} (Figure S2c, Supporting Information). When compared with GO, G band of graphene sheets shifts to a low-wavelength range, indicating a significant decrease of oxygen-containing groups on the graphene backbone. In addition, as shown in the UV-vis absorption spectra (Figure S2d, Supporting Information), a marked red-shift of the typical peak of graphene sheets (corresponding transition of aromatic C=C) is found in comparison with GO. This result suggests that the electronic conjugation of GO was restored after the removal of oxygen-containing groups, which is in agreement with previous reports.[31] Based on above analysis, the graphene sheets in the reduced coagulations not only form a 3D graphene framework, but also have a high reduction level, certainly resulting in a high electrical conductivity for the as-prepared graphene-based composites (see below).

2.3. Electrical Properties of the Graphene-Based Nanocomposites

The obtained reduced coagulations, which consist of GSs and PS nanospheres, were hotly pressed to films for electrical conductivity measurement. The graphene-polymer composites are a typical electrical percolation system. For such a system, the conductive filler forms an infinite network of conductive paths through the insulation matrix in the vicinity of the percolation threshold (ρ_c), leading to a rapid increase in the electrical conductivity of the composite (σ). The relation between σ and ρ_c obeys a power law:

$$\sigma = \sigma_0[(\rho - \rho_c)(1 - \rho_c)]^t \text{ for } \rho > \rho_c \quad (1)$$

where σ_0 is the conductivity of the filler, ρ the filler volume fraction, and t is a critical exponent.[22]

Figure 5 shows the conductivity variation of the graphene-polystyrene composites as a function of graphene volume fraction, which can be described by the power law in Equation (1). Percolation in the composites does occur when the graphene concentration, ρ, is near 0.15 vol%. This electrical percolation threshold is quite low, suggesting a good dispersion of GSs in the polymer matrix. However, this value is slightly higher than that of the composites with isocyanate-treated GSs, possibly because of wave-structure of GSs in the matrix, which arises from electrostatic interactions between GO and polymer nanospheres. Remarkably, the conductivity of our composites rapidly rises over a 2.5 vol% range, and is up to 259.9 S/m at a loading of 2.2 vol%. An increase in GS loading beyond 2.5 vol% yields a more gradual increase in electrical conductivity, showing value of 607.1 S/m at 3.5 vol% and 1083.3 S/m at 4.8 vol%. For comparison, the graphene and carbon nanotube-polymer composites were fabricated by the solution mixing methods. As shown in **Figure 6**a, the electrical conductivity of these composites is at least one order of magnitude lower than that of the composites fabricated by a self-assembly and hot press process.

Currently, high electrically conductive graphene-based polymer composites were mainly fabricated via the solution mixing methods by using functional GSs.[38,39] After a careful comparison, we find that the electrical conductivity of our composites is higher than the highest value reported in the literature[39] and some representative results are shown in **Table 1**. The high electrical conductivity in our samples can certainly be attributed to the following two factors. One factor is a 3D compactly interconnected graphene network constructed in the polymer matrix. In order to observe the morphology of these 3D graphene networks, the testing samples with 4.8 vol% GSs were annealed at high temperature under nitrogen atmosphere to obtain the residual graphene skeleton. Figure 6b–e shows

© 2013 WILEY-VCH Verlag GmbH & Co. KGaA, Weinheim

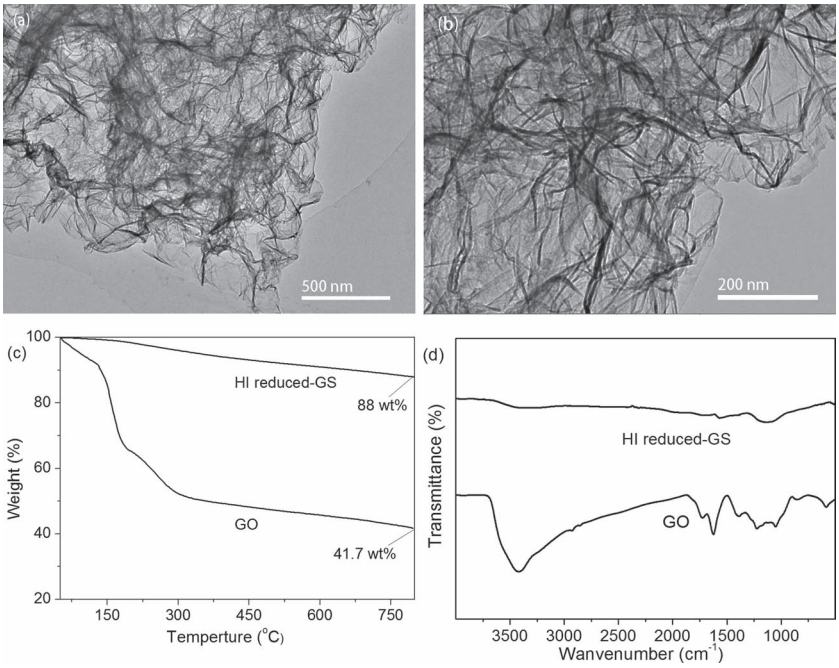

Figure 4. a,b) Typical TEM images of the 3D graphene networks. c) TGA curves and d) FT-IR spectra of GO and HI reduced-GS (the collapsed graphene framework).

the representative SEM images of the graphene skeleton. We can see that there exist foam-like networks with a 3D compactly interconnected graphene structure, suggesting that GSs were uniformly dispersed in the polymer matrix. Notably, the hot-press process is critical to generate compact junction contact between GSs in the 3D architecture. A comparison between electrical conductivity of the composite films before versus after hot-press process is given in Figure S3, Supporting Information. The conductivity of the films after hot-press is about three times higher than that of the films without undergoing the hot-press process.

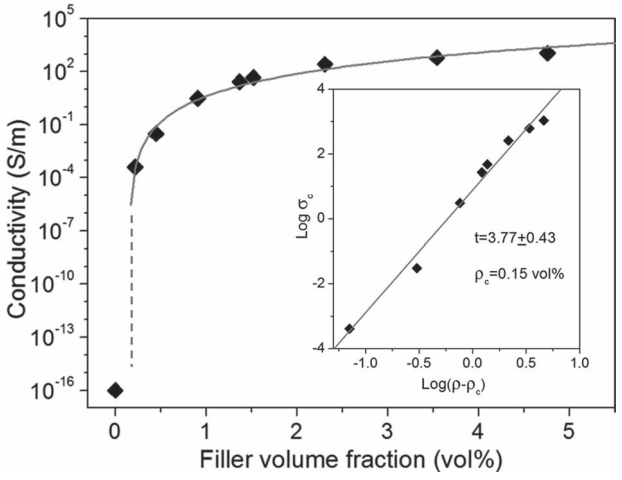

Figure 5. Electrical conductivity of the graphene-based polystyrene composites as a function of filler volume fraction.

Another key factor is high reduction level of GO by using HI solution in our preparation approach, which makes the integrated GSs show a high electrical conductivity. In the previous study,[40,41] it has been demonstrated that the graphene films show higher electrical conductivity with increasing the reduction level. For comparison, hydrazine, a conventional reducing agent for reduction of GO, was used to reduce GO in the composite preparation process. The conductivity of the resulting composite films is much lower than that of the films via the HI reduction (Figure S4c, Supporting Information). The GSs extracted from the composite films remain more functional groups when compared with the HI-reduced GSs, which is confirmed by TGA and FT-IR (Figure 4 and Figure S4, Supporting Information) curves.

Figure S5a (Supporting Information) shows a 3D structured graphene paper, which is obtained by annealing the film with 2.2 vol% GSs at high temperature. The conductivity of the paper can be up to 707 S/m, higher than that of the composite film (259.9 S/m). The higher electrical conductivity should be attributed to the deeper removal of the functional groups from the GSs during the annealing process of the composite film. Figure S5b–d (Supporting Information) shows the cross-sectional SEM images of the graphene paper, a porous 3D network is observed. This porous structure can prevent the agglomeration of GSs. The high conductivity and porous structure satisfy the critical features for high performance electrode materials of batteries and supercapacitors.[13,42,43] Thus, this graphene paper may have potential applications for energy storage.

For practical applications, the mechanical and thermal properties of the obtained graphene-polystyrene composites are required to be taken into account. The mechanical property was evaluated by the elastic modulus data of the composites, as shown in Figure S6, Supporting Information. The elastic modulus significantly increases with increasing the graphene content within a volume fraction of 4.8 vol%. The highest modulus is up to 2045 Mpa for the composite with 4.8 vol% graphene, approximately two fold higher than that of the pure PS. The modulus enhancement is associated to the unique 3D graphene network in the PS composites. In the 3D structure, the GSs can be uniformly distributed in the matrix. Moreover, there exists van der Walls and π–π interactions between GS and PS macromolecules. The combination of these two factors leads to an effective load transfer from the matrix to GSs. In addition, the two factors also restrict the thermal molecular motion of the PS chains, resulting in a shift in glass transition temperatures (Tgs) toward the higher values. The dramatic impact of GS on the Tgs of the composites is given in Figure S7, Supporting Information. The Tgs of the composites increase from 83.3 to 99.5 °C when the volume fraction is increased from 0 to 4.8%. Such a thermal behavior is consistent with results

© 2013 WILEY-VCH Verlag GmbH & Co. KGaA, Weinheim

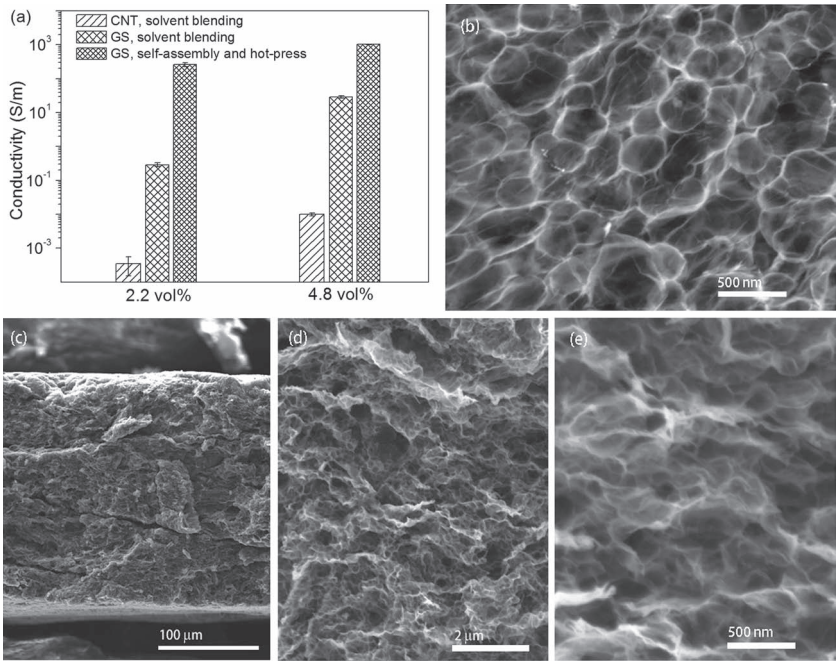

Figure 6. a) Electrical conductivity comparison of the graphene and carbon nanotube- polystyrene composites fabricated by the solution mixing and electrostatic self-assembly methods. b) Top view and c–e) cross-sectional SEM images of the remained graphene skeleton after annealing the testing samples at high temperature under nitrogen atmosphere.

reported previously for the functionalized graphene-based polymer composites.[44,45]

The future development of mutifuncitonal flexible electronics such as sensor and actuators presents new challenges for designing and fabricating light-weight, flexible, and highly conductive films. In this study, we replaced the PS emulsion with a commercial EVA microemulsion, which can serve as a source of polymer matrixes for the production of flexible conductive films via the similar procedure. As shown in **Figure 7**a, the photograph demonstrates the high degree of flexibility of the composite thin film with 2.2 vol% GSs. Figure 7b,c displays the SEM images of the corresponding reduced coagulation consisting of GS and EVA microspheres. Almost all the microspheres are encapsulated and connected by flexible GSs. The EVA film after hot press, similar to the PS films, also contains a 3D graphene skeleton (Figure 7d–f), thus resulting in a high electrical conductivity. The conductivity of the EVA-graphene film is up to 209 S/m with a graphene loading of 2.2 vol%.

3. Conclusions

We have developed a self-assembly and hot press technique for the fabrication of the polymer composites with 3D interconnected graphene networks. The compact contact between GSs in the 3D architecture and high reduction level of GSs render the composites outstanding electrical conductivity, which is superior to that of the reported composites with chemically functional GSs at the same loading. A 3D porous graphene framework obtained by annealing the composite film shows higher electrical conductivity when compared with the composite, possibly having potential applications including electrode materials for lithium ion batteries and supercapacitors. Moreover, the self-assembly and hot press technique is a general strategy for fabrication of graphene-based composites with different polymer matrixes, including PS and flexible EVA matrixes. It should be noted that

Table 1. Electrical conductivity of the graphene-based polymer composites.

Polymer matrix	Graphene type	Processing	Percolation threshold	Highest conductivity	Ref.
PS	Functionalized GSs	Solvent blending	0.1 vol%	1 S/m at 2.5 vol%	[22]
PS	Functionalized GSs	Solvent blending	0.1 vol%	4.19 S/m at 4.19 vol%	[10]
PET[a)]	Functionalized GSs	Melt compouding	0.47 vol%	2.1 S/m at 3.0 vol%	[32]
Polycarbonate	Functionalized GSs	Emulsion blending	0.14 vol%	51.2 S/m at 2.2 vol%	[33]
Cellulose	Chemically converted GSs	Solvent blending	0.3 wt%	71.8 S/m at 10 wt% (≈4.8 vol%)	[34]
Polyurethane	Functionalized GSs	Solvent blending	–	30 S/m at 10 wt% (≈4.8 vol%)	[35]
VVC[a)]	Chemically converted GSs	Solvent blending	0.15 vol%	≈0.01 S/m at 3.5 vol%	[30]
Chitosan	Chemically converted GSs	Solvent blending	–	1.2 S/m at 6.0 wt% (≈2.2 vol%)	[36]
PS	Functionalized GSs	Solvent blending	–	≈2 S/m at 2.0 vol%	[37]
PS	GSs	Self-assembly and hot-press	0.15 vol%	259.9 S/m at 2.2 vol%; 1024.8 S/m at 4.8 vol%	Present work

[a)]PET and VVC are polyethylene terephthalate and vinyl chloride/vinyl acetate copolymer, respectively.

© 2013 WILEY-VCH Verlag GmbH & Co. KGaA, Weinheim

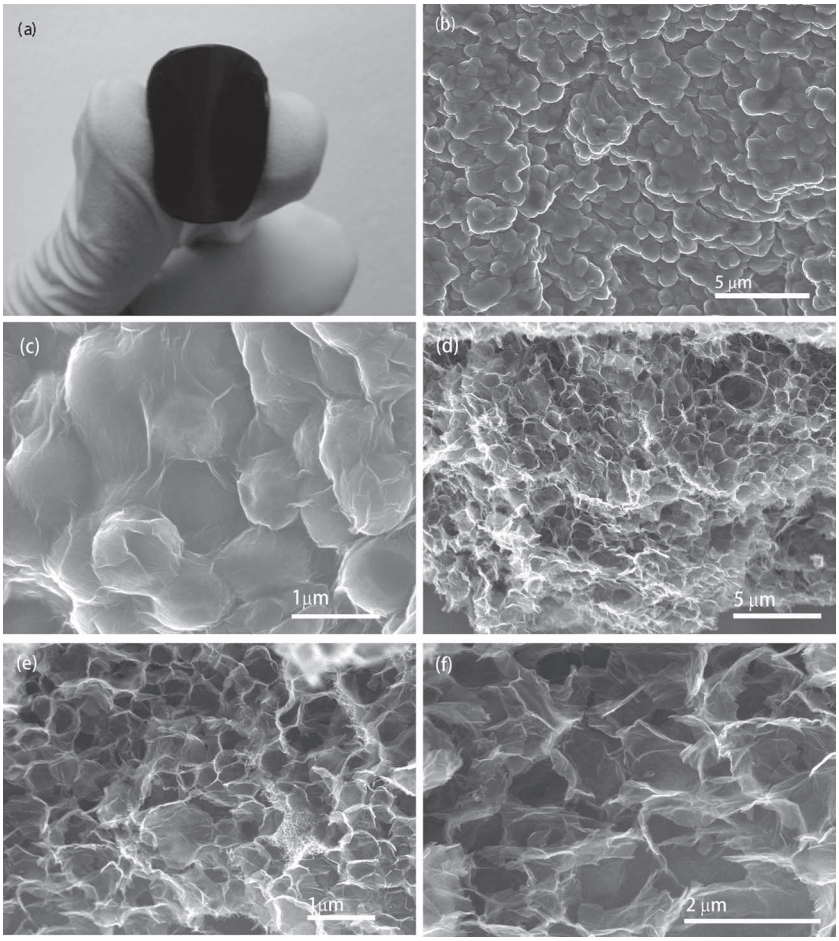

Figure 7. a) Digital photograph of the EVA film with 2.2 vol% GSs, showing the flexibility of the film. b,c) Typical SEM images of the reduced coagulation consisting of EVA microspheres and GSs. d,e) Cross-sectional SEM images of the remained graphene skeleton after removal of the EVA matrix at high temperature under nitrogen atmosphere.

the self-assembly process are performed in aqueous phase, an environment-friendly condition. We believe that such a simple and effective technique will provide a new pathway for the large-scale production of various highly conductive polymer composites for practical applications.

4. Experimental Section

Materials: Natural graphite powder (30 μm with purity > 99.85%) was purchased from Sinapharm Chemical Reagent co., Ltd, China. Graphene oxide was synthesized from natural graphite powder by a modified Hummers method, the details of which have been described elsewher.[24] Carbon nanotubes (diameter: 8–15 nm, Lengh: 50 mm) were received from Chengdu Organic Chemicals Co, Ltd., Chinese Academy of Sciences. EVA emulsion was purchased from Shanghai kunsheng bond co., Ltd, China.

Synthesis of Amino-Modified Polystyrene Nanospheres: Polystyrene nanospheres were synthesized by emulsion polymerization. In a typical process, the poly(vinylpyrrolidone) stabilizer (0.76 g) was firstly dissolved in 30 mL deionized water. Then, styrene monomer (3.9 g) and ammonium persulfate (0.5 g) were added into the solution. Subsequently, the obtained mixture was purged with nitrogen to eliminate the inhibiting effect of oxygen, and then heated to 70 °C with vigorous magnetic stirring. After reaction for 8 h, the desired polystyrene nanospheres were obtained by washing with methanol and centrifugal separation.

The resultant polystyrene nanospheres were further dispersed in 50 mL deionized water via sonication. 16 mL concentrated nitric acid and 6 mL concentrated sulfuric acid were add into the solution. After reaction at 45 °C for 12 h, the product was obtained with deionized water and centrifugal separation. Subsequently, the obtained product was dispersed in 50 mL NaOH solution (2 mol/L), and then NaS_2O_4 powder (2 g) was added into the solution. After reaction at 75 °C for 4 h. the amino-modified polystyrene nanospheres were obtained by washing with deionized water and centrifugal separation.

Fabrication of the Composites with 3D Interconnected Graphene Networks: In a typical process, for the composites with low loading of graphene (<2.0 vol%), 50 mL amino-modified polystyrene nanosphere dispersion (4 mg/mL) and 50 mL aqueous graphene oxide suspension(a desired concentration) were simultaneously added dropwise into a 150 mL flask under the magnetic stirring. After 0.5 h, the coagulation of the polymer composites was isolated via filtration, washed with deionized water, and then immersed into 50 mL HI solution (50 wt%) at 90 °C for 24 h to reduce graphene oxide. For comparison, the hydrazine solution (20 mL hydrazine in 50 mL water) was used to reduce graphene oxide. The reduced coagulation was collected via filtration and washed with deionized water 3 times. The obtained product was hotly pressed to platelets at 110 °C for testing their electrical conductivity. For the composites with high loading of graphene (>2 vol%), 200 mL amino-modified polystyrene nanosphere dispersion (1.0 mg/mL) and 200 mL aqueous graphene oxide suspension (a desired concentration) were simultaneously added dropwise into a 1 L flask under vigorous magnetic stirring. The following process is similar to that of fabricating the composite with low loading of graphene. Similar to above process, ethylene vinyl actate (EVA) microspheres were used to fabricate flexible conductive films with the composites with a 3D interconnected graphene network. It should be noted that the hot press process for EVA films was carried out at 90 °C.

Preparation of the Carbon Nanotube and Graphene-Based Composites by Solvent Blending: A desired amount of carbon nanotubes or graphene sheets was dispersed in 20 mL DMF by ultrasonic treatment. Graphene sheets were prepared via reducing graphene oxide in HI solution (50 wt%). At the same time, a certain amount of polystyrene (Dow Chemical, STYRON666H) was dissolved in 20 mL DMF solution at 60 °C. Then, the two solutions were mixed and stirred for 5 min. Subsequently, the resulting mixture was added into a large volume of deionized water to obtain the agglomeration of the polymer composites. The composite powder was collected by separation, washing by deionized water, and drying. Finally, the obtained powder was hotly pressed into film for electrical conductivity measurement.

Characterization: The morphology and microstructure of the samples were investigated by FE-SEM (nanoSEM 230, NOVA, USA), TEM (JEM-2010, JEOL, Japan), AFM (IMODE NANOSCOPE, DI, USA), XRD (D/max-2200/PC, Rigaku, Japan), Roman (LabRam HR800, Jobin Yvon, France), and UV-vis (Lambda 20, Perkin Elmer, USA). Thermogravimetric analysis (TGA-209F3, NETZSCH, Germany) was carried out under a 20 mL/min N_2 purge at a heating rate of 10 °C/min from room temperature to 800 °C. Differential scanning calorimetry (DSC-200F3, NETZSCH, Germany) was employed to measure glass transition temperature of the

© 2013 WILEY-VCH Verlag GmbH & Co. KGaA, Weinheim

composites, which was conducted by heating the samples at 10 °C/min from room temperture to 200 °C. Zeta potential measurements were performed using a Zetasizer 3000 (Malvern Instruments). The graphene oxide and polystyrene nanosphere samples were diluted to 0.10 and 1.0 mg/mL respectively before measurements. The pH values of graphene oxide and nanosphere dispersions were adjusted by adding ammonia solution or hydrochloric acid. The electric conductivity of the samples was measured by a four-probe method. Mechanical property tests were conducted using an INSTRON 4465 Electromechanical Tester with a crosshead speed of 2 mm/min at room temperature.

Supporting Information

Supporting information is available from the Wiley Online Library or from the author.

Acknowledgements

X.Y.H. and P.K.J. acknowledge the supports from the Research Fund for the Doctoral Program of Higher Education (Grant No. 20100073120038), the National Science Foundation of China (No. 51107081), the SJTU Undergraduate Innovative Test Program (s110IPP003007) and the Shanghai Leading Academic Discipline Project (Grant No. B202). C.W. and X.Y.H. are grateful to researchers in the instrument analysis center of Shanghai Jiao Tong University for their help in material analysis.

Received: May 6, 2012
Revised: June 12, 2012
Published online: September 12, 2012

[1] T. Sekitani, Y. Noguchi, K. Hata, T. Fukushima, T. Aida, T. Someya, *Science* **2008**, *321*, 1468.
[2] K. Y. Chun, Y. Oh, J. Rho, J. H. Ahn, Y. J. Kim, H. R. Choi, S. Baik, *Nat. Nanotechnol.* **2010**, *5*, 853.
[3] S. Nambiar, J. T. W. Yeow, *Biosens. Bioelectron.* **2011**, *26*, 1825.
[4] Y. Hu, W. Chen, L. H. Lu, J. H. Liu, C. R. Chang, *ACS Nano* **2010**, *4*, 3498.
[5] H. M. Kim, K. Kim, C. Y. Lee, J. Joo, S. J. Cho, H. S. Yoon, D. A. Pejakovic, J. W. Yoo, A. J. Epstein, *Appl. Phys. Lett.* **2004**, *84*, 589.
[6] H. Kim, A. A. Abdala, C. W. Macosko, *Macromolecules* **2010**, *43*, 6515.
[7] A. K. Geim, *Science* **2009**, *324*, 1530.
[8] F. He, S. Lau, H. L. Chan, J. T. Fan, *Adv. Mater.* **2009**, *21*, 710.
[9] H. J. Salavagione, G. Martinez, G. Ellis, *Macromol. Rapid Commun.* **2011**, *32*, 1771.
[10] N. Liu, F. Luo, H. X. Wu, Y. H. Liu, C. Zhang, J. Chen, *Adv. Funct. Mater.* **2008**, *18*, 1518.
[11] F. Liu, S. Y. Song, D. F. Xue, H. J. Zhang, *Adv. Mater.* **2012**, *24*, 1089.
[12] Y. X. Xu, K. X. Sheng, C. Li, G. Q. Shi, *ACS Nano* **2010**, *4*, 4324.
[13] S. H. Lee, D. H. Lee, W. J. Lee, S. O. Kim, *Adv. Funct. Mater.* **2011**, *21*, 1338.
[14] Z. P. Chen, W. C. Ren, L. B. Gao, B. L. Liu, S. F. Pei, H. M. Cheng, *Nat. Mater.* **2011**, *10*, 424.
[15] J. N. Coleman, *Adv. Funct. Mater.* **2009**, *19*, 3680.
[16] J. M. Englert, A. Hirsch, X. L. Feng, K. Mullen, *Angew. Chem. Int. Ed.* **2011**, *50*, A17.
[17] B. Luo, S. M. Liu, L. J. Zhi, *Small* **2012**, *8*, 630.
[18] M. Segal, *Nat. Nanotechnol.* **2009**, *4*, 611.
[19] C. Wu, X. Y. Huang, G. L. Wang, X. F. Wu, K. Yang, S. T. Li, P. K. Jiang, *J. Mater. Chem.* **2012**, *22*, 7010.
[20] C. P. Song, D. Q. Wu, F. Zhang, P. Liu, Q. H. Lu, X. L. Feng, *Chem. Commun.* **2012**, *48*, 2119.
[21] D. Li, M. B. Muller, S. Gilje, R. B. Kaner, G. G. Wallace, *Nat. Nanotechnol.* **2008**, *3*, 101.
[22] S. Stankovich, D. A. Dikin, G. H. B. Dommett, K. M. Kohlhaas, E. J. Zimney, E. A. Stach, R. D. Piner, S. T. Nguyen, R. S. Ruoff, *Nature* **2006**, *442*, 282.
[23] S. Park, R. S. Ruoff, *Nat. Nanotechnol.* **2009**, *4*, 217.
[24] C. Wu, X. Huang, L. Xie, X. Wu, J. Yu, P. Jiang, *J. Mater. Chem.* **2011**, *21*, 17729.
[25] O. C. Compton, B. Jain, D. A. Dikin, A. Abouimrane, K. Amine, S. T. Nguyen, *ACS Nano* **2011**, *5*, 4380.
[26] S. Stankovich, D. A. Dikin, R. D. Piner, K. A. Kohlhaas, A. Kleinhammes, Y. Jia, Y. Wu, S. T. Nguyen, R. S. Ruoff, *Carbon* **2007**, *45*, 1558.
[27] G. Williams, B. Seger, P. V. Kamat, *ACS Nano* **2008**, *2*, 1487.
[28] T. Kuilla, S. Bhadra, D. Yao, N. H. Kim, S. Bose, J. H. Lee, *Prog. Polym. Sci.* **2010**, *35*, 1350.
[29] D. Vuluga, J. M. Thomassin, I. Molenberg, I. Huynen, B. Gilbert, C. Jerome, M. Alexandre, C. Detrembleur, *Chem. Commun.* **2011**, *47*, 2544.
[30] T. Wei, G. L. Luo, Z. J. Fan, C. Zheng, J. Yan, C. Z. Yao, W. F. Li, C. Zhang, *Carbon* **2009**, *47*, 2296.
[31] D. V. Kosynkin, A. L. Higginbotham, A. Sinitskii, J. R. Lomeda, A. Dimiev, B. K. Price, J. M. Tour, *Nature* **2009**, *458*, 872.
[32] H. B. Zhang, W. G. Zheng, Q. Yan, Y. Yang, J. W. Wang, Z. H. Lu, G. Y. Ji, Z. Z. Yu, *Polymer* **2010**, *51*, 1191.
[33] M. Yoonessi, J. R. Gaier, *ACS Nano* **2010**, *4*, 7211.
[34] N. D. Luong, N. Pahimanolis, U. Hippi, J. T. Korhonen, J. Ruokolainen, L. S. Johansson, J. D. Nam, J. Seppala, *J. Mater. Chem.* **2011**, *21*, 13991.
[35] H. K. He, C. Gao, *Chem. Mater.* **2010**, *22*, 5054.
[36] X. L. Wang, H. Bai, Z. Y. Yao, A. R. Liu, G. Q. Shi, *J. Mater. Chem.* **2010**, *20*, 9032.
[37] W. J. Li, X. Z. Tang, H. B. Zhang, Z. G. Jiang, Z. Z. Yu, X. S. Du, Y. W. Mai, *Carbon* **2011**, *49*, 4724.
[38] H. Bai, C. Li, G. Q. Shi, *Adv. Mater.* **2011**, *23*, 1089.
[39] J. R. Potts, D. R. Dreyer, C. W. Bielawski, R. S. Ruoff, *Polymer* **2011**, *52*, 5.
[40] T. F. Yeh, F. F. Chan, C. T. Hsieh, H. S. Teng, *J. Phys. Chem. C* **2011**, *115*, 22587.
[41] X. J. Zhou, J. L. Zhang, H. X. Wu, H. J. Yang, J. Y. Zhang, S. W. Guo, *J. Phys. Chem. C* **2011**, *115*, 11957.
[42] M. F. El-Kady, V. Strong, S. Dubin, R. B. Kaner, *Science* **2012**, *335*, 1326.
[43] L. Wei, M. Sevilla, A. B. Fuertes, R. Mokaya, G. Yushin, *Adv. Funct. Mater.* **2012**, *22*, 827.
[44] T. Ramanathan, A. A. Abdala, S. Stankovich, D. A. Dikin, M. Herrera-Alonso, R. D. Piner, D. H. Adamson, H. C. Schniepp, X. Chen, R. S. Ruoff, S. T. Nguyen, I. A. Aksay, R. K. Prud'homme, L. C. Brinson, *Nat. Nanotechnol.* **2008**, *3*, 327.
[45] M. Fang, K. G. Wang, H. B. Lu, Y. L. Yang, S. Nutt, *J. Mater. Chem.* **2009**, *19*, 7098.

© 2013 WILEY-VCH Verlag GmbH & Co. KGaA, Weinheim